K_v1.3 induced hyperpolarisation is required for efficient Kaposi's sarcoma-associated herpesvirus lytic replication

Holli Carden[1], Katherine L. Harper[1], Timothy J. Mottram[1], Oliver Manners[1], Katie L. Allott[1], Mark L. Dallas[2], David J. Hughes[3], Jonathan D. Lippiat[4], Jamel Mankouri[1] & Adrian Whitehouse[1,5,*]

[1]*School of Molecular and Cellular Biology and Astbury Centre for Structural Molecular Biology, University of Leeds, Leeds, LS2 9JT, United Kingdom*

[2]*School of Pharmacy, University of Reading, Reading RG6 6AP, United Kingdom*

[3]*Biomedical Sciences Research Complex, School of Biology, University of St Andrews, North Haugh, St Andrews, KY16 9ST*

[4]*School of Biomedical Sciences, Faculty of Biological Sciences, University of Leeds, Leeds, LS2 9JT, United Kingdom*

[5]*Department of Biochemistry and Microbiology, Rhodes University, Grahamstown 6140, South Africa*

*Correspondence: Adrian Whitehouse, a.whitehouse@leeds.ac.uk Tel: +44 (0)113 343 7096

One-sentence summary: K_v1.3 is required for KSHV lytic replication

Keywords:

KSHV; antiviral; ion channel; K_v1.3; NFAT; lytic replication.

Abstract

Understanding the host factors critical for virus replication can identify new targets for therapeutic intervention. Using pharmacological and genetic silencing approaches, we showed that the oncogenic herpesvirus, Kaposi's sarcoma-associated herpesvirus (KSHV) requires a B cell expressed voltage-gated K^+ channel, $K_v1.3$, to enhance lytic replication. We showed that the KSHV replication and transcription activator (RTA) protein upregulates $K_v1.3$ expression, leading to enhanced K^+ channel activity and hyperpolarisation of the B cell membrane. Enhanced $K_v1.3$ activity then promoted intracellular Ca^{2+} influx, leading to the Ca^{2+} driven nuclear localisation of the KSHV replication and transcription activator (RTA) and host NFAT proteins and the subsequent NFAT1-responsive gene expression., KSHV lytic replication and infectious virion production could be inhibited by $K_v1.3$ blockers or through $K_v1.3$ silencing. These findings provide mechanistic insight into the essential role of host ion channels during KSHV infection and highlight $K_v1.3$ as a druggable host factor that is key to the successful completion of KSHV lytic replication.

Introduction

Ion channels are multi-subunit, pore-forming membrane proteins that control the rapid and selective passage of ions across the plasma membrane and the membranes of subcellular organelles (*1*). As such, ion channels have a wide variety of roles in controlling the ion homeostasis of the cell and its organelles, action potential firing, membrane potential and cell volume. Given this wide range of functions and their ubiquitous nature, impairment of channel function whether be an increase or loss of activity, have been implicated in a variety of disorders and diseases known as channelopathies (*2*) and may also play an important role in enhancing cell proliferation and invasion of tumour cells. Several stages of virus replication cycles, including virion entry, virus egress and the maintenance of an environment conducive to virus replication have been in-part, suggested to be dependent on the ability of virus proteins to manipulate ion channel activity (*2, 3*). This is reinforced by observations that pharmacological modulation of virus-targeted ion channels can impede virus replication, highlighting ion channels as promising candidates for host targeted anti-viral therapeutics. Some of these ion-channel blocking drugs are in widespread human use for ion channel-related diseases, highlighting new potential for drug repurposing.

Kaposi's sarcoma-associated herpesvirus (KSHV) is a gamma 2-herpesvirus directly linked to the development of Kaposi's sarcoma (KS), a highly vascular tumour of endothelial lymphatic origin, and several other AIDS-associated malignancies including primary effusion lymphoma (PEL) and some forms of multicentric Castleman's disease (MCD) (*4-7*). KSHV exhibits a biphasic life cycle consisting of latent persistence or lytic replication (*8*). In contrast to other oncogenic herpesviruses in which latent gene expression drives tumorigenesis, both the latent and lytic replication phases are essential for KSHV-mediated tumorigenicity (*9*). Latency is established in B cells and in the tumour setting, where viral gene expression is limited to the latency-associated nuclear antigen (LANA), viral FLICE inhibitory protein, viral cyclin, kaposins and several virally-encoded miRNAs (*10-12*). Upon reactivation, KSHV enters the lytic replication phase, leading to the highly orchestrated expression of more than 80 viral proteins that are sufficient for the production of infectious virions (*13, 14*). In KS lesions, most infected

66 cells harbour the virus in a latent state. However, a small proportion of cells undergo lytic replication
67 that leads to the secretion of angiogenic, inflammatory and proliferative factors that act in a paracrine
68 manner on latently-infected cells to enhance tumorigenesis (*15*). Lytic replication also enhances
69 genomic instability (*16*) and sustains KSHV episomes in latently-infected cells that would otherwise be
70 lost during cell division (*17*). The ability to inhibit the lytic replication phase therefore represents a
71 therapeutic intervention strategy for the treatment of KSHV-associated diseases (*18, 19*).

72 The transition from latent infection to lytic replication is controlled by both host and viral
73 factors (*20, 21*). These factors converge on the interaction between the latency associated nuclear
74 antigen (LANA) and the master regulator of the latent-lytic switch, KSHV replication and transcription
75 activator (RTA) protein (*22*). Notably, agents that mobilize intracellular Ca^{2+} can induce the expression
76 of KSHV-RTA and enhance KSHV reactivation and lytic replication (*23*), however this activity can be
77 blocked with inhibitors of calcineurin-dependent signal transduction (*24*). Cytoplasmic concentrations
78 of Ca^{2+} are increased by a network of ion channels and transporters (*25*) To date, a specific role for
79 host cell ion channels during the lytic replication stage of KSHV or any herpesvirus have yet to be fully
80 defined. B lymphocytes, the primary site of KSHV latent infection, are regulated by a network of
81 transporters and ion channels that control the cytoplasmic concentrations of calcium (Ca^{2+}),
82 magnesium (Mg^{2+}) and zinc (Zn^{2+}), which act as important second messengers to regulate critical B cell
83 effector functions (*26*). The repertoire of ion channels in B cells include potassium (K^+) channels, Ca^{2+}
84 channels, P2X receptors and transient receptor potential (TRP) channels, in addition to Mg^{2+} and Zn^{2+}
85 transporters. To-date, a role for these channels during KSHV infection has not been described.

86 Here, we performed a systematic analysis of the role of host ion channels during the KSHV
87 lytic replication phase in a range of KSHV-infected cells, including modified B cell lymphoma cells and
88 primary HUVEC cells, to reveal avenues for host-directed therapeutic intervention. Using a
89 combination of electrophysiological and biochemical approaches, we showed that KSHV activates a
90 voltage-gated K^+ channel $K_v1.3$, the pharmacological and genetic silencing of which inhibits KSHV lytic
91 replication. We further defined the mechanism for this dependence by showing that $K_v1.3$ activation

leads to hyperpolarisation induced Ca^{2+} influx, which enhanced the nuclear localisation of the KSHV replication and transcription activator (RTA) and host NFAT proteins, which in turn was required to drive virus replication. We therefore demonstrate the essential role of the $K_v1.3$ channel in the lytic replication cycle of a herpesvirus.

Results

K^+ channels are required for efficient KSHV reactivation

K^+ channels represent the largest family of ion channels with over 70 genes identified in the human genome (*27*). We first sought to determine if their activity is required for efficient KSHV lytic replication. Here virus reactivation assays were performed in the presence of potassium chloride (KCl) to collapse cellular K^+ channel gradients, or the broad spectrum K^+ channel blockers, barium chloride ($BaCl_2$), tetraethylammonium (TEA) and quinidine (Qn). All inhibitors used in this study were assessed at non-toxic concentrations measured by MTS assays during both latent and lytic phases (**Figure S1A-M**). KSHV reactivation was assessed in TREx BCBL1-RTA cells, a latently infected KSHV B-lymphocyte cell line that expresses a Myc-tagged viral RTA under the control of a doxycycline-inducible promoter. Upon analysis, TREx BCBL1-RTA cells reactivated for 24 h in the presence of each K^+ channel inhibitor showed a drastic reduction in the expression of early ORF57, delayed early ORF59 and the late minor capsid (mCapsid) ORF65 proteins (**Figure 1A, Figure S2A**). No such reduction was observed in the expression of Myc-RTA or GAPDH, highlighting specific effects on lytic replication as opposed to dox-induced RTA induction. These data indicated a requirement for K^+ channel function during the KSHV lytic replicative cycle.

We next investigated the molecular identity of the specific K^+ channel(s) required for KSHV lytic replication to reveal more specific drug targets. K^+ channels can be divided into subfamilies of voltage-gated K^+ channels (K_v), calcium-activated K^+ channels (K_{Ca}), inwardly rectifying K^+ channels (K_{ir}) and two-pore domain K+ channels (K2P) channels. We found that treatment with 4-aminopyridine (4-AP), a non-selective K_v blocker, led to a concentration-dependent reduction in lytic replication (**Figure 1B, Figure S2B**), suggestive of a role for K_v channels during lytic induction. Electrophysiological studies have identified an array of functional K_v channels expressed within B lymphocytes, with a member of the *Shaker* related family, $K_v1.3$, most extensively characterised (*28*). When specific $K_v1.3$ blockers margatoxin (MgTX) and ShK-Dap^{22} were included in our reactivation assays, a concentration-

dependent reduction of ORF57 protein production was observed (**Figure 1C-D, Figure S2C-D**). In contrast, incubation in the presence of TRAM-34 or Senicapoc, both blockers of B lymphocyte $K_{Ca}3.1$ channels, showed no effect on lytic ORF57 protein production in TREx BCBL1-RTA cells (**Figure 1E-F, Figure S2E-F**). ShK-Dap[22] also reduced the expression of various temporally-expressed KSHV lytically expressed genes (**Figure S3A-C**) and inhibited KSHV lytic replication in other KSHV-infected cell lines, namely BCBL-1 (**Figure S3D-E**) and iSLK cells (**Figure S3F-G**). Furthermore, infectious virions harvested from reactivated TREx BCBL1-RTA cells were used to re-infect Human Umbilical Vein Endothelial Cells (HUVEC) in the absence or presence of ShK-Dap[22]. HUVEC cells reinfected in the presence of ShK-Dap[22] showed a ~90% reduction in viral *ORF57* mRNA expression compared to control cells (**Figure S3H**). Together this suggested that $K_v1.3$ is essential for KSHV lytic replication.

To confirm a role for $K_v1.3$ during KSHV lytic replication, TREx BCBL1-RTA cells were stably transduced with lentivirus-based shRNAs depleting $K_v1.3$ expression by over 85% (**Figure S4A-C**). Reactivation assays showed that $K_v1.3$ silencing led to a significant reduction in ORF57, ORF59 and ORF65 protein levels compared to control (**Figure 1G-H, Figure S2G-H**). To examine whether the depletion of $K_v1.3$ also influenced infectious virus production, supernatants of reactivated TREx BCBL1-RTA cells were used to re-infect naive cells and KSHV infection was determined by qRT-PCR or LANA expression. Cells reinfected with supernatants from $K_v1.3$ depleted cells showed a ~80% reduction in viral *ORF57* mRNA compared to control cells (**Figure 1I**) and a dramatic reduction in LANA-immunostaining (**Figure 1J**). To ensure our $K_v1.3$ depletion studies were not due to off-target effects of $K_v1.3$ shRNAs, complementation assays were performed using a lentivirus expressing a $K_v1.3$ shRNA resistant expression construct. Results show that this construct rescued KSHV lytic replication and infectious virion production in the $K_v1.3$ depleted cell line, as measured by ORF57 protein production (**Figure 1H, Figure S2H**) and LANA immunostaining of reinfected supernatants (**Figure 1J**). Together, these data confirmed that KSHV requires B cell $K_v1.3$ channel activity to undergo efficient lytic replication and infectious virus production.

KSHV enhances K_v1.3 expression and activity

As KSHV is dependent on K_v1.3 to complete its lytic replication cycle, its ability to modulate K_v1.3 activity was next investigated. qRT-PCR and immunoblotting analysis showed that K_v1.3 expression increased in TREx BCBL1-RTA cells undergoing lytic replication compared to latent cells (**Figure 2A, Figure S2I**). In contrast, qRT-PCR analysis showed that *K_{Ca}3.1* expression decreased during KSHV lytic replication, likely due to KSHV SOX-mediated host cell shutoff (*29*) (**Figure 2B**). To elucidate whether the increase in K_v1.3 expression led to enhanced K^+ efflux mediated by K_v1.3 channels during lytic replication, whole-cell patch clamp analysis was performed. Electrophysiological recordings revealed a voltage-gated outward K^+ current present in latent TREx BCBL1-RTA cells that was significantly enhanced in cells undergoing lytic replication (**Figure 2C**). To conclusively determine that K_v1.3 channels were responsible for these changes, recordings were repeated in the presence of ShK-Dap^{22}, which led to a dramatic inhibition of the K^+ current during lytic replication (**Figure 2C**). A similar reduction was observed in cells depleted for K_v1.3 using lentivirus-based shRNAs, compared to control (**Figure 2D**). Notably, we also observed that reactivated TREx BCBL1-RTA cells exhibited a significantly more hyperpolarised membrane compared to latent cells, which was reversed upon K_v1.3 depletion (**Figure 2E**). Results also suggested that K_v1.3 depletion resulted in a slightly increased negative membrane potential that control latent cells, the reasons for this are unknown, but it must be noted that hyperpolarisation is not to the extent observed upon lytic reactivation of control cells. Membrane hyperpolarisation was also confirmed using a membrane potential-sensitive dye, bis (1,3-dibutylbarbituric acid) trimethine oxonol; $DiBAC_4(3)$. Results showed a time-dependent decrease in fluorescence intensity in control cells undergoing the early stages of lytic replication, consistent with enhanced membrane hyperpolarization, whereas no reduction in $DiBAC_4(3)$ fluorescence was observed in K_v1.3 depleted cells (**Figure 2F**). As a further control, addition of the calcium ionophore A23187, which induces depolarisation, enhanced $DiBAC_4(3)$ fluorescence (**Figure 2F**). Together these results demonstrated that KSHV lytic replication increases K_v1.3 expression, resulting in enhanced K_v1.3 currents and membrane hyperpolarisation during lytic KSHV replication.

KSHV RTA mediates the upregulation of K_v1.3 during lytic replication

We next investigated the mechanism by which KSHV enhances K_v1.3 currents. Given that membrane hyperpolarisation was observed as early as 4 h post-reactivation (**Figure 2F**), we examined whether KSHV-encoded early proteins were sufficient to induce *K_v1.3* expression and activation. A549 and U87 cells were transiently transfected with control GFP, RTA-GFP or ORF57-GFP expression constructs and *K_v1.3* transcript levels were assessed by qRT-PCR at 24 h post-transfection. We found that RTA-GFP alone was sufficient to induce *K_v1.3* expression at the transcript level in a dose-dependent manner (**Figure 3A-B**), confirming KSHV RTA transcriptional activator as the direct inducer of K_v1.3 expression.

Specificity Protein (SP) 1 functions as a co-adapter for RTA-mediated transactivation and has been shown to increase K_v1.3 expression (*30*). To further dissect the relationship between KSHV RTA and K_v1.3, we examined a potential cooperative role for SP1 during the upregulation of K_v1.3 during KSHV lytic replication. RTA-GFP transfections were performed in the presence of Mithramycin A, a selective SP1 inhibitor that displaces SP1 binding from its target promoter (*31*). Results showed Mithramycin A treatment suppressed the RTA-mediated increase in *K_v1.3* expression (**Figure 3C**), but had little effect on the RTA-mediated upregulation of the IL-6 promoter, suggestive of an in-direct mechanism whereby SP1 recruits RTA to the K_v1.3 promoter. ChIP assays further confirmed an association of both RTA and SP1 with the K_v1.3 promoter, which significantly increased during lytic replication (**Figure 3D**). Together, these data revealed KSHV RTA as the key driver of K_v1.3 expression during the KSHV lytic cycle.

K_v1. 3 induced membrane hyperpolarisation provides the driving force for Ca^{2+} influx required for KSHV reactivation

In B lymphocytes, $K_v1.3$ maintains a hyperpolarised membrane potential that is necessary to sustain the driving force for Ca^{2+} entry. $K_v1.3$ therefore indirectly modulates an array of Ca^{2+}-dependent cellular processes in B cells. To assess the role of $K_v1.3$ during lytic replication, we assayed Ca^{2+} influx into control and $K_v1.3$-depleted TREx BCBL1-RTA cells during the KSHV lytic cycle using the ratiometric Ca^{2+} dye Fura-Red and flow cytometry analysis. We observed an increase in cytoplasmic Ca^{2+} over a 24 h period of lytic reactivation in control cells, that was absent in $K_v1.3$-depleted TREx BCBL1-RTA cells (**Figure 4A, Figure S5A**). Based on these data, we next investigated whether Ca^{2+} influx defines the requirement of $K_v1.3$ for efficient lytic replication. To this end, we examined what effect Ca^{2+} depletion, by EGTA chelation, had on KSHV lytic replication. Results showed that Ca^{2+} depletion prevented the nuclear import and increased cytoplasmic accumulation of the KSHV RTA transactivating protein (**Figure 4B**), leading to a corresponding reduction in lytic gene expression (**Figure 4C, Figure S5B-D**)**.** Conversely we also assessed what mimicking Ca^{2+} influx had on KSHV lytic replication, here TREx BCBL1-RTA cells were reactivated in the absence or presence of the Ca^{2+} ionophore A23187. Results show that the presence of A23187 enhanced lytic ORF57 protein levels compared to control cells (**Figure 4D, Figure S2J**), which aligns with previous findings (*23*). We next determined whether addition of the calcium ionophore had the ability to recover KSHV lytic replication in a $K_v1.3$ depleted cell line. Notably, lytic ORF57 protein production was observed in $K_v1.3$ depleted cells upon A23187 addition, suggesting that the calcium ionophore could override the dependence of KSHV on $K_v1.3$ (**Figure 4E, Figure S2K**). Together, these data suggested that Ca^{2+} influx is essential for efficient KSHV lytic replication and is induced by $K_v1.3$-mediated hyperpolarisation.

KSHV-mediated Ca^{2+} influx initiates NFAT1 nuclear localisation and NFAT1-mediated gene expression

Ca^{2+} influx can initiate multiple signalling pathways, including the serine/threonine phosphatase calcineurin and its target transcription factor NFAT (nuclear factor of activated T cells) (*25*). The phosphatase activity of calcineurin is activated through binding of the Ca^{2+}-calmodulin

complex, displacing the calcineurin autoinhibitory domain from the active site of the enzyme. Dephosphorylation of cytoplasmic NFAT proteins by calcineurin unmasks their nuclear localization sequences, leading to nuclear translocation and NFAT-responsive gene expression. We therefore determined whether the calcineurin-mediated nuclear import of NFAT1 was important for KSHV lytic replication. Results showed that in the presence of the calcineurin/NFAT1 inhibitors, cyclosporin A (CsA) and VIVIT, a dose-dependent reduction in KSHV ORF57 protein production (**Figure 5A-B Figure S2L-M**), and a reduction in KSHV lytic gene expression was observed (**Figure S6A-B**).

We next investigated whether KSHV-mediated hyperpolarisation and Ca^{2+} influx promoted the nuclear translocation of NFAT, by comparing its nuclear/cytoplasmic distribution in latent versus lytic TREx BCBL1-RTA cells using immunofluorescence analysis. Results showed that NFAT1 translocates to the nucleus upon KSHV lytic reactivation, but remains cytoplasmic during latent infection (**Figure 5C**). The nuclear localisation of NFAT1 was found to be dependent on $K_v1.3$-mediated hyperpolarisation as it was prevented by ShK-Dap[22] (**Figure 5C**), in addition it was also dependent on calcineurin activity, since NFAT1 nuclear localisation was also inhibited in the presence of CsA (**Figure 5C**). Consistent with the enhanced nuclear localisation of NFAT, we observed an increase in NFAT-responsive gene expression during KSHV lytic replication, which was reduced upon $K_v1.3$ depletion compared to control cells (**Figure 5D**). A number of NFAT-responsive genes, such as COX-2, FGF2 and ANGPT2 have been shown to be upregulated during KSHV infection and have been implicated in KSHV-mediated pathogenesis (*32-34*). Together, these data suggested that the KSHV-induced hyperpolarisation mediated by $K_v1.3$ and the subsequent influx of Ca^{2+}, enhances the nuclear localisation of NFAT1 and induces NFAT-driven gene expression (**Figure 6**).

Discussion

KSHV infection is responsible for various malignancies, including KS, PEL and some cases of MCD. These diseases are highly associated with compromised immune function, and as such represent some of the most common cancers in areas of the world where HIV infection is prevalent (*4*). Notably, KS is the most common cancer in many sub-Saharan countries. Therefore, understanding the molecular mechanisms that underlie KSHV biology is of the utmost importance if developing targeted therapeutic approaches. KSHV latency-associated viral proteins have been well characterised in transformation and tumourigenesis pathways; however, it is clear that KSHV also requires the lytic phase to drive tumourigenesis (*18, 35*). This is supported by a number of studies showing abrogation of KSHV gene expression impairs KSHV-associated oncogenesis. This is also emphasised by successful treatment of KS patients with drugs that inhibit KSHV replication, indicating that the lytic phase is required for both the initiation of KS and the maintenance of disease (*36*). Lytic genes encode angiogenic and KS growth factors which stimulate the proliferation of latently-infected cells and angiogenesis in a paracrine manner. Lytic replication can also replenish episomes lost within highly proliferating tumour cells, maintaining viral latency in select cell populations. Discovery of both the viral and cellular determinants that control lytic induction can therefore inform new therapeutic targets for anti-KSHV drug discovery. This is particularly important in light of the increasing number of AIDS-associated, Iatrogenic and classic KS cases (*37*) due to the increased survival rates of AIDS patients, the higher success rates of transplant surgery, and increasing global life expectancy (*38*).

Ion channels control a range of cellular processes that are known to be co-opted by viruses (*2, 3*). Accordingly, ion channels have emerged as druggable host targets to prevent both RNA and DNA viruses from the successful completion of their life cycles (*39*). Given the known dependence of KSHV lytic replication on Ca^{2+} signalling (*24*), coupled to previous studies demonstrating the ability of VZV and HSV-1 to activate Na^{+} and Ca^{2+} family members (*40, 41*), we specifically investigated the role of B cell expressed ion channels during KSHV lytic reactivation, using a range of KSHV-infected cells including modified lymphoma cells and primary HUVEC cells. Using known pharmacological ion

channel modulators, genetic silencing approaches and electrophysiological analysis, we showed that KSHV requires a B-cell expressed voltage-gated K^+ channel, $K_v1.3$, to enhance lytic replication. We showed that the KSHV RTA protein upregulates $K_v1.3$ expression via indirect SP1-mediated transactivation. Enhanced $K_v1.3$ expression and activity led to hyperpolarisation of the B-cell membrane potential, initiating Ca^{2+} influx and the resulting Ca^{2+} driven nuclear localisation of NFAT1 to complete the KSHV lytic replication cycle. In addition, we highlighted that $K_v1.3$-mediated Ca^{2+} influx is also required for efficient nuclear import of the KSHV latent–lytic transactivator, RTA, which is essential to drive lytic replication. At present, it is thought that the role of Ca^{2+} in RTA-mediated nuclear import may involve the enhanced recruitment of nuclear import proteins, or the unmasking of nuclear localisation signals (*42*). Together, this revealed that $K_v1.3$ is a direct contributor to KSHV lytic replication (**Figure 6**).

A striking feature of KSHV is the homology of its numerous ORFs to cellular genes (*14*). These virus-encoded proteins contribute to KSHV-associated pathogenesis by subverting cell signalling pathways, including interferon-regulated anti-viral responses, cytokine-regulated cell growth, cell cycle progression and apoptosis. Many viruses encode viroporins (*43*); ion channel proteins that modulate the ionic milieu of intracellular organelles to control virus protein stability and trafficking. However, no known viroporins exist amongst the ORFs of KSHV and it is therefore likely that evolution has tailor-made its proteins to regulate the expression of host cell ion channels to induce the Ca^{2+} signalling required for both latent and lytic replicative phases. Tumorigenesis may represent a by-product of this regulation, since in an array of human cancers, $K_v1.3$ expression is enhanced and correlates with the grade of tumour malignancy (*44*). It is also noteworthy that features of KS tumours mirror the phenotypic effects of $K_v1.3$ overexpression, including the enhanced expression of inflammatory and angiogenic cytokines and uncontrolled cell cycle progression. This may reveal the KSHV driven activation of $K_v1.3$ as a channelopathy, a group of diseases characterised by altered function of ion channel proteins or their regulatory subunits. Several ion channel inhibitors either comprise small organic molecules, such as quinine and 4AP, or peptides purified from venom (*30, 45*).

297 These venom-derived peptides are highly stable and resist denaturation due to the disulphide bridges
298 formed within the molecules (*45*). As with margatoxin, most are derived from scorpion venom, such
299 as agitoxins, kaliotoxin, maurotoxin and noxiustoxin yet many inhibitors have been derived from ShK,
300 a peptide originally isolated from the sea anemone *Stichodactyla helianthus* (*46*). Given the
301 abundance of natural sources for K_v1.3-inhibition a safe, effective therapeutic based on these
302 compounds is a promising target for prevention. Additionally, it is interesting to note that the anti-
303 CD20 monoclonal antibody rituximab, which promotes Kv1.3 channel inactivation via FcγRIIB
304 receptors (*39*), substantially improves the outcome of KSHV patients (*47*).

305 Finally, K_v channels have been previously identified as a restriction factor to the entry of both
306 Hepatitis C virus (*48*) and Merkel cell polyomavirus (*49*), through their abilities to inhibit endosome
307 acidification-mediated viral membrane fusion. Whilst the inhibition of endosomal acidification has
308 been shown to reduce the entry and trafficking of KSHV virions, our electrophysiological analysis
309 revealed enhanced cell surface K_v1.3 activity during lytic replication that directly contributed to the
310 hyperpolarised membrane potential of cells that was required for efficient KSHV replication. Thus,
311 whilst additional roles of K_v1.3 in endosomes cannot be excluded, our data suggested a divergent role
312 of K_v1.3 during herpesvirus infection that may be cell-type and/or virus specific.
313

Materials and Methods

Cell Culture

TREx-BCBL-1-RTA cells (kindly provided by Prof. Jae Jung, University of Southern California) are a BCBL-1-based primary effusion lymphoma (PEL) B cell line engineered to express exogenous Myc-tagged RTA upon addition of doxycycline, triggering reactivation of the KSHV lytic cycle. BCBL1 cells were a gift from Dr Andrew Hislop (University of Birmingham, UK). A549 and HEK-293T cell lines were purchased from the American Type Culture Collection (ATCC). HUVECs (Lonza), were a kind gift from Dr Lia Pinto (University of Leeds), U-87 MG cells (kindly provided by Prof. J. Ladbury, University of Leeds) are a human brain glioblastoma astrocytoma cell line. iSLK-BAC16 cells (also provided by Prof. Jae Jung, University of Southern California) are a Caki1-derived renal carcinoma cell line, latently infected with bacterial artificial chromosome 16 (BAC16)-derived KSHV. A549, iSLK, U87 and HEK-293T cells were grown in DMEM (Life Technologies) supplemented with 10% foetal calf serum (FCS) (Life Technologies) and 1% penicillin/streptomycin (P/S). TREx BCBL1-RTA and BCBL1 cells were grown in RPMI 1640 medium (Life Technologies) supplemented with 10% FCS and 1% P/S, TREx BCBL1-RTA were maintained under hygromycin B (Life Technologies) selection (100 µg/ml). HUVECs were grown in EGM-2 Endothelial cell growth medium-2 Bullet kit (Lonza). All cell lines tested negative for mycoplasma. Reactivation into the KSHV lytic cycle was induced using 2 µg/ml doxycycline hyclate, (Sigma) for TREx BCBL1-RTA or with 2 mM sodium butyrate and 20 ng/ml 2-O-tetradecanoylphorbol-13-acetate (TPA) (both Sigma). All cells were maintained at 37°C in a humidified incubator with 5% CO_2.

Antibodies, Plasmids and Transient Transfections

Antibodies used in western blotting are listed in Supplementary Table S1. Primers used for depletion studies and qRT-PCR are listed in Supplementary Table 2. pVSV.G and psPAX2 were a gift from Dr Edwin Chen (University of Westminster, London). PLKO.1 TRC cloning vector was purchased from

Addgene (gift from David Root; Addgene plasmid #10878). psiCheck2 was a gift from Dr James Boyne (Leeds Beckett University). GFP, GFP-ORF50 and GFP-ORF57 have been described previously (*50*) (*51*). Plasmid transfections were performed using Lipofectamine 2000 (Life Technologies), at a ratio of 2 ug plasmid to 4 ul Lipofectamine in 100 ul opti-MEM. Transfection media was incubated at room temperature for 15 minutes before 1x 10^6 cells were treated, dropwise. Cells were harvested after 24 hours.

Lentivirus-based shRNA Knockdown and Rescue

Lentiviruses were generated by transfection of HEK-293T cells seeded in 12-well plates using a three-plasmid system. Per 6-well, 4 µl of lipofectamine 2000 (Thermo Scientific) were used together with 1 µg of pLKO.1 plasmid expressing shRNA against the protein of interest (Dharmacon), 0.65 µg of pVSV.G, and 0.65 µg psPAX2. Eight hours post-transfection, media was changed with 2 mL of DMEM supplemented with 10% (v/v) FCS. 500,000 TREx BCBL1-RTA cells in 6 well plates were infected by spin inoculation with the filtered viral supernatant for 60 min at 800 x g at room temperature, in the presence of 8 µg/mL of polybrene (Merck Millipore). Virus supernatants were removed 7 h post-spin inoculation and cells were maintained in fresh growth medium for 48 h prior to selection in 3 µg/mL puromycin (Sigma-Aldrich). Stable cell lines were generated after 8 days of selection. All shRNA plasmids were purchased from Dharmacon. Scramble shRNA was a gift from Professor David Sabatini (Addgene plasmid # 1864). K_v1.3 codon exchange plasmids were generated via inverse PCR mutagenesis utilising a pLENTI-CMV-K_v1.3-ZEO plasmid generated via Gibson Assembly. The mutagenesis process involved exchanging the wobble base of each codon of the 20bp targeted by the shRNA constitutively expressed within the cells. Thus, the resulting K_v1.3 RNA transcripts show resistance to shRNA activity, restoring expression in transfected cells. The plasmids were transfected in to the ΔKv1.3 TREx-BCBL1-RTA cell line following the three-plasmid system described above, with the shRNA-resistant pLENTI-CMV-K_v1.3-ZEO plasmid replacing the pLKO.1 plasmid, and zeomycin used for selection at 250 µg/ml.

Immunofluorescence

Cells were cultured overnight on poly-L-lysine (Life Technologies) coated glass coverslips in 24-well plates. Cells were fixed with 4% paraformaldehyde (Calbiochem) for 10 min and permeabilised with 0.1% Triton X-100 for 20 min. Cells were blocked in PBS containing 1% BSA for 1 h at 37°C and labelled with primary antibodies for 1 h at 37°C. Cells were washed five times with PBS and labelled with appropriate secondary antibodies for 1 h at 37°C. Cells were washed five times with PBS and mounted in VECTASHIELD containing DAPI (Vector Labs) (*52*). Images were obtained using a Zeiss LSM880 Inverted Microscope confocal microscope and processed using ZEN 2009 imaging software (Carl Zeiss) (*53*).

Electrophysiology

TREx BCBL1-RTA cells seeded onto poly-L-lysine (Life Technologies) coated glass coverslips and were transferred to a recording chamber, containing 140 mM NaCl, 5 mM KCl, 2 mM $MgCl_2$, 10 mM HEPES-NaOH, pH 7.2, 2 mM $CaCl_2$, 10 mM glucose, and mounted on the stage of a Nikon Eclipse inverted microscope. Patch pipettes (5–8 MΩ) were filled with a solution consisting of: 140 mM KCl, 5 mM EGTA, 2 mM $MgCl_2$, 1 mM $CaCl_2$, 10 mM HEPES KOH, pH 7.2, 10 mM glucose. Voltage-clamp recordings were performed, in the absence and presence of ShK-Dap^{22} dissolved in dH_20, using a HEKA EPC-10 integrated patch clamp amplifier controlled by Patchmaster software (HEKA). Series resistance was monitored after breaking into the whole cell configuration. To examine K^+ currents, a series of depolarizing steps were performed from −100 to +60 mV in 10 mV increments for 100 ms. Resting membrane potential was measured using the current clamp mode of the amplifier. Results are shown as the mean ± SEM of n number of individual cells. Statistical analysis was performed using an unpaired Student's T test. $p<0.05$ was considered statistically significant.

Flow Cytometry

Bis-(1,3-Dibutylbarbituric Acid) Trimethine Oxonol ($DiBAC_4(3)$) and Fura Red (both ThermoFisher) were added to cells at a final concentration of 1 µM in RPMI-media. Cells were incubated at 37°C with Fura Red for 30 min or $DiBAC_4(3)$ for 5 min and washed in PBS. Cells were analysed on a CytoFLEX Flow Cytometer (Beckman). Data were quantified using CytExpert software (Beckman) as previously described (*54*).

Proliferation (MTS) assays

Cellular viability in the presence of inhibitor compounds used (Appendix Table S1) was determined using non-radioactive CellTiter 96 AQueous One Solution Cell Proliferation Assay (MTS) reagent (Promega), according to the manufacturer's recommendations (*53*). TREx BCBL1-RTA cells (~20,000) were seeded in triplicate in a flat 96-well tissue culture plates (Corning) and treated with the indicated inhibitors for 24 h. CellTiter 96 AQueous One Solution Reagent was added to the cells for 1 h at 5% CO_2, 37^{O}C. Absorbances were measured at 490 nm using an Infinite plate reader (Tecan).

Two-step quantitative reverse transcription PCR (qRT-PCR)

Total RNA was extracted using the Monarch® Total RNA Miniprep Kit (New England Biolabs) as per the manufacturer's protocol. RNA (1 µg) was diluted in a total volume of 16 µl nuclease-free water, and 4 µl LunaScript RT SuperMix (5X) (New England Biolabs) was added to each sample. Reverse transcription was performed using the protocol provided by the manufacturer. cDNA was stored at -20°C, RNA was stored at -80°C. Quantitative PCR (qPCR) reactions (20 µl) included 1X SensiMix SYBR green master mix (Bioline), 0.5 µM of each primer and 5 µl template cDNA (used at 1:200 dilution in RNase-free water). Cycling was performed in a RotorGene Q instrument (Qiagen) (*53*). The cycling programme was a 10 min initial preincubation at 95°C, followed by 40 cycles of 95°C for 15 sec, 60°C for 30 sec and 72°C for 20 sec. After qPCR, a melting curve analysis was performed between 65°C and 95°C (with 0.2°C increments) to confirm amplification of a single product. To assess primer amplification efficiency (AE), for each gene of interest a standard curve was constructed using a pool

of cDNA derived from unreactivated and reactivated cells. At least four different dilutions of pool cDNA were quantified to generate a standard curve. The slope of the standard curve was used to calculate the AE of the primers using the formula: AE = (10−1/slope). For gene expression analysis all genes of interest were normalised against the housekeeping gene GAPDH (ΔCT). A summary of all the primers used in this study is provided in Supplementary Table 2.

Chromatin immunoprecipitation (ChIP)

Formaldehyde-crosslinked chromatin was prepared using the Pierce Chromatin Prep Module (Thermo Scientific) following the manufacturer's protocol. Cells (2 x 10^6) were digested with six units of micrococcal nuclease (MNase) per 100 µl of MNase Digestion buffer in a 37°C water bath for 15 min. These conditions resulted in optimal sheared chromatin with most fragments ranging from 150–300 base pairs in size. Immunoprecipitations were performed using EZ-ChIP kit (Millipore) kits overnight at 4°C and contained 50 µl of digested chromatin (2 x 10^6 cells), 450 µl of ChIP dilution buffer and 1.5 µg of RNAPII antibody (clone CTD4H8) (Millipore) or isotype antibody, normal mouse IgG (Millipore). qPCR reactions were performed using either 2 µl of immunoprecipitated DNA or 2 µl of input DNA as template.

Immunoblotting

Protein samples were separated on SDS-PAGE gels as previously described (*55*), and transferred to nitrocellulose membranes (Amersham) via semi-dry transfer using a Trans-Blot® Turbo™ blotter (BioRad). Membranes were blocked in TBS + 0.1% Tween 20 and 5% dried skimmed milk powder and probed with relevant primary antibodies followed by horseradish peroxidase (HRP)-conjugated polyclonal goat anti-mouse and polyclonal goat anti-rabbit secondary antibodies (Dako). Membranes were treated with EZ-ECL (Geneflow) and imaged using a G-Box (Syngene).

Quantification and statistical analysis

Statistical analysis as specified in figure legends were performed with Prism 9 (GraphPad software Inc., San Diego, California, United States). When differences between two groups were analysed, unpaired Student's t test was used; when differences between more than two groups were analysed, the one-way unpaired analysis of variance (ANOVA) corrected for multiple comparisons using Tukey's multiple comparison test was used. Graphs with multiple time points were analysed with a simple linear regression. A p value <0.05 was considered significant ($*$ for $p < 0.05$, $**$ for $p < 0.01$ and $***$ for $p < 0.001$).

References

1. B. Brown, H. Nguyen, H. Wulff, Recent advances in our understanding of the structure and function of more unusual cation channels [version 1; peer review: 2 approved]. *F1000Research* **8**, (2019).
2. F. W. Charlton *et al.*, Ion Channels as Therapeutic Targets for Viral Infections: Further Discoveries and Future Perspectives. *Viruses* **12**, (2020).
3. S. Hover, B. Foster, J. N. Barr, J. Mankouri, Viral dependence on cellular ion channels - an emerging anti-viral target? *J Gen Virol* **98**, 345-351 (2017).
4. D. Ganem, KSHV and the pathogenesis of Kaposi sarcoma: listening to human biology and medicine. *Journal of Clinical Investigation* **120**, 939-949 (2010).
5. D. P. Dittmer, B. Damania, Kaposi's Sarcoma-Associated Herpesvirus (KSHV)-Associated Disease in the AIDS Patient: An Update. *Cancer Treat Res* **177**, 63-80 (2019).
6. P. Lange, B. Damania, Kaposi Sarcoma-Associated Herpesvirus (KSHV). *Trends Microbiol* **28**, 236-237 (2020).
7. M. He *et al.*, Molecular Biology of KSHV in Relation to HIV/AIDS-Associated Oncogenesis. *Cancer Treat Res* **177**, 23-62 (2019).
8. J. C. Murphy *et al.*, Kaposi's sarcoma-associated herpesvirus induces specialised ribosomes to efficiently translate viral lytic mRNAs. *Nat Commun* **14**, 300 (2023).
9. L. Giffin, B. Damania, KSHV: pathways to tumorigenesis and persistent infection. *Adv Virus Res* **88**, 111-159 (2014).
10. D. Dittmer *et al.*, A cluster of latently expressed genes in Kaposi's sarcoma-associated herpesvirus. *Journal of Virology* **72**, 8309-8315 (1998).
11. K. A. Staskus *et al.*, Kaposi's sarcoma-associated herpesvirus gene expression in endothelial (spindle) tumor cells. *J Virol* **71**, 715-719 (1997).
12. L. V. McClure, C. S. Sullivan, Kaposi's sarcoma herpes virus taps into a host microRNA regulatory network. *Cell Host Microbe* **3**, 1-3 (2008).
13. G. Broussard, B. Damania, Regulation of KSHV Latency and Lytic Reactivation. *Viruses* **12**, (2020).
14. C. Arias *et al.*, KSHV 2.0: a comprehensive annotation of the Kaposi's sarcoma-associated herpesvirus genome using next-generation sequencing reveals novel genomic and functional features. *PLoS Pathog* **10**, e1003847 (2014).
15. J. Nicholas, Human herpesvirus 8-encoded proteins with potential roles in virus-associated neoplasia. *Frontiers in Bioscience* **12**, 265-281 (2007).
16. B. R. Jackson, M. Noerenberg, A. Whitehouse, A Novel Mechanism Inducing Genome Instability in Kaposi's Sarcoma-Associated Herpesvirus Infected Cells. *PLoS Pathog* **10**, e1004098 (2014).
17. A. Grundhoff, D. Ganem, Inefficient establishment of KSHV latency suggests an additional role for continued lytic replication in Kaposi sarcoma pathogenesis. *J Clin Invest* **113**, 124-136 (2004).
18. O. Manners, J. C. Murphy, A. Coleman, D. J. Hughes, A. Whitehouse, Contribution of the KSHV and EBV lytic cycles to tumourigenesis. *Curr Opin Virol* **32**, 60-70 (2018).
19. D. J. Hughes, J. J. Wood, B. R. Jackson, B. Baquero-Perez, A. Whitehouse, NEDDylation is essential for Kaposi's sarcoma-associated herpesvirus latency and lytic reactivation and represents a novel anti-KSHV target. *PLoS Pathog* **11**, e1004771 (2015).
20. K. K. Aneja, Y. Yuan, Reactivation and Lytic Replication of Kaposi's Sarcoma-Associated Herpesvirus: An Update. *Front Microbiol* **8**, 613 (2017).
21. D. M. Lukac, Y. Yuan, in *Human Herpesviruses: Biology, Therapy, and Immunoprophylaxis,* A. Arvin *et al.*, Eds. (Cambridge, 2007).
22. P. Purushothaman, P. Dabral, N. Gupta, R. Sarkar, S. C. Verma, KSHV Genome Replication and Maintenance. *Front Microbiol* **7**, 54 (2016).

23. J. Chang, R. Renne, D. Dittmer, D. Ganem, Inflammatory cytokines and the reactivation of Kaposi's sarcoma-associated herpesvirus lytic replication. *Virology* **266**, 17-25 (2000).
24. J. P. Zoeteweij *et al.*, Targeted inhibition of calcineurin signaling blocks calcium-dependent reactivation of Kaposi sarcoma-associated herpesvirus. *Blood* **97**, 2374-2380 (2001).
25. G. R. Crabtree, S. L. Schreiber, SnapShot: Ca2+-calcineurin-NFAT signaling. *Cell* **138**, 210-210.e211 (2009).
26. T. Mahtani, B. Treanor, Beyond the CRAC: Diversification of ion signaling in B cells. *Immunological Reviews* **291**, 104-122 (2019).
27. M. S. P. Sansom *et al.*, Potassium channels: structures, models, simulations. *Biochimica et Biophysica Acta (BBA) - Biomembranes* **1565**, 294-307 (2002).
28. H. Wulff, H.-G. Knaus, M. Pennington, K. G. Chandy, K⁺ Channel Expression during B Cell Differentiation: Implications for Immunomodulation and Autoimmunity. *The Journal of Immunology* **173**, 776 (2004).
29. B. Glaunsinger, D. Ganem, Lytic KSHV infection inhibits host gene expression by accelerating global mRNA turnover. *Mol Cell* **13**, 713-723 (2004).
30. S. H. Jang *et al.*, Nuclear localization and functional characteristics of voltage-gated potassium channel Kv1.3. *J Biol Chem* **290**, 12547-12557 (2015).
31. R. Liu *et al.*, Mithramycin A suppresses basal triple-negative breast cancer cell survival partially via down-regulating Krüppel-like factor 5 transcription by Sp1. *Scientific Reports* **8**, 1138 (2018).
32. F. C. Ye *et al.*, Kaposi's sarcoma-associated herpesvirus promotes angiogenesis by inducing angiopoietin-2 expression via AP-1 and Ets1. *J Virol* **81**, 3980-3991 (2007).
33. N. Sharma-Walia *et al.*, NFAT and CREB regulate Kaposi's sarcoma-associated herpesvirus-induced cyclooxygenase 2 (COX-2). *J Virol* **84**, 12733-12753 (2010).
34. L. Wang *et al.*, The Kaposi's sarcoma-associated herpesvirus (KSHV/HHV-8) K1 protein induces expression of angiogenic and invasion factors. *Cancer Res* **64**, 2774-2781 (2004).
35. K. L. Harper *et al.*, Dysregulation of the miR-30c/DLL4 axis by circHIPK3 is essential for KSHV lytic replication. *EMBO Rep*, e54117 (2022).
36. N. Coen, S. Duraffour, R. Snoeck, G. Andrei, KSHV Targeted Therapy: An Update on Inhibitors of Viral Lytic Replication. *Viruses* **6**, (2014).
37. E. Rohner *et al.*, HHV-8 seroprevalence: a global view. *Systematic Reviews* **3**, 11 (2014).
38. J. T. King, A. C. Justice, M. S. Roberts, C.-C. H. Chang, J. S. Fusco, Long-Term HIV/AIDS Survival Estimation in the Highly Active Antiretroviral Therapy Era. *Medical Decision Making* **23**, 9-20 (2003).
39. K. Wang, S. Xie, B. Sun, Viral proteins function as ion channels. *Biochim Biophys Acta* **1808**, 510-515 (2011).
40. L. Ding *et al.*, T-type calcium channels blockers inhibit HSV-2 infection at the late stage of genome replication. *Eur J Pharmacol* **892**, 173782 (2021).
41. P. G. Kennedy *et al.*, Varicella-zoster viruses associated with post-herpetic neuralgia induce sodium current density increases in the ND7-23 Nav-1.8 neuroblastoma cell line. *PLoS One* **8**, e51570 (2013).
42. A. Sarma, W. Yang, Calcium regulation of nucleocytoplasmic transport. *Protein Cell* **2**, 291-302 (2011).
43. C. Scott, S. Griffin, Viroporins: structure, function and potential as antiviral targets. *J Gen Virol* **96**, 2000-2027 (2015).
44. A. Teisseyre, A. Palko-Labuz, K. Sroda-Pomianek, K. Michalak, Voltage-Gated Potassium Channel Kv1.3 as a Target in Therapy of Cancer. *Front Oncol* **9**, 933 (2019).
45. S. Bajaj, J. Han, Venom-Derived Peptide Modulators of Cation-Selective Channels: Friend, Foe or Frenemy. *Frontiers in Pharmacology* **10**, 58 (2019).
46. M. W. Pennington *et al.*, Development of highly selective Kv1.3-blocking peptides based on the sea anemone peptide ShK. *Mar Drugs* **13**, 529-542 (2015).

47. T. S. Uldrick *et al.*, Rituximab plus liposomal doxorubicin in HIV-infected patients with KSHV-associated multicentric Castleman disease. *Blood* **124**, 3544-3552 (2014).
48. J. Mankouri *et al.*, Suppression of a pro-apoptotic K⁺ channel as a mechanism for hepatitis C virus persistence. *Proceedings of the National Academy of Sciences* **106**, 15903 (2009).
49. S. J. Dobson, J. Mankouri, A. Whitehouse, Identification of potassium and calcium channel inhibitors as modulators of polyomavirus endosomal trafficking. *Antiviral Research* **179**, 104819 (2020).
50. F. Gould, S. M. Harrison, E. W. Hewitt, A. Whitehouse, Kaposi's sarcoma-associated herpesvirus RTA promotes degradation of the Hey1 repressor protein through the ubiquitin proteasome pathway. *Journal of virology* **83**, 6727-6738 (2009).
51. S. Schumann *et al.*, Targeting the ATP-dependent formation of herpesvirus ribonucleoprotein particle assembly as an antiviral approach. *Nat Microbiol* **2**, 16201 (2016).
52. M. A. Calderwood, K. T. Hall, D. A. Matthews, A. Whitehouse, The herpesvirus saimiri ORF73 gene product interacts with host-cell mitotic chromosomes and self-associates via its C terminus. *J Gen Virol* **85**, 147-153 (2004).
53. B. Baquero-Pérez, A. Whitehouse, Hsp70 Isoforms Are Essential for the Formation of Kaposi's Sarcoma-Associated Herpesvirus Replication and Transcription Compartments. *PLOS Pathogens* **11**, e1005274 (2015).
54. N. Nwogu *et al.*, Cellular sheddases are induced by Merkel cell polyomavirus small tumour antigen to mediate cell dissociation and invasiveness. *PLoS Pathog* **14**, e1007276 (2018).
55. D. J. Goodwin *et al.*, The carboxy terminus of the herpesvirus saimiri ORF 57 gene contains domains that are required for transactivation and transrepression. *Journal of General Virology* **81**, 2253-2658 (2000).

Acknowledgements

We thank Professor Jae Jung, University of Southern California School of Medicine, Los Angeles, for the TREx BCBL1-RTA cells, Dr Lia Pinto, University of Leeds for HUVECs, Prof. J. Ladbury, University of Leeds for U87 cells and Dr Edwin Chen, University of Westminster for the lentivirus vectors. KSHV ORF59 antibody was a kind gift from Prof. Britt Glaunsinger (University of California, Berkeley).

Funding

This work was supported by a Rosetrees Trust PhD studentship, M662, White Rose BBSRC Doctoral Training Partnership in Mechanistic Biology (95519935), BBSRC project grant (BB/T00021X/1) and a Royal Society University Research Fellowship, G:480764 (Mankouri).

Author Contributions

Conceptualization (JM, AW); Data curation (HC, KLH, TJM, OM, KLA, MLD, DJH); Formal Analysis (HC, MLD, DJH, KLH, TJM, OM, KLA, JDL, JM, AW); Funding acquisition (AW, JM); Investigation (HC, KLH, TJM, OM, MLD, DJH); Writing – original draft (HC, JM, AW); Writing – review & editing (All authors).

Disclosure and Competing Interests Statement

The authors declare no conflicts of interest.

Data and Materials Availability

All data needed to evaluate the conclusions in the paper are present in the paper or the Supplementary Materials. This paper does not report original code. Any additional information required to reanalyze the data reported in this paper is available from the lead contact upon request.

Figure Legends

Figure 1. K_v1.3 channels are required for efficient KSHV lytic replication.

(A-E) TREx BCBL1-RTA cells remained unreactivated or were pre-treated with non-cytotoxic concentrations of (A) general K^+ inhibitors prior to reactivation with doxycycline hyclate, or increasing amounts of (B) 4AP (C) MgTX, (D) ShK-Dap[22], (E) TRAM34 and (F) Senicapoc. Cell lysates were then probed with either ORF57-, ORF59- or ORF65-specific antibodies. GAPDH was used as a measure of equal loading (n=3 biologically independent samples).

(G) Control and K_v1.3-depleted cells lines were reactivated with doxycycline hyclate. Cell lysates were probed with Myc-, ORF57-, ORF59- or ORF65-specific antibodies and GAPDH used as a measure of equal loading (n=3 biologically independent samples).

(H) Control, K_v1.3-depleted or K_v1.3-rescued cell lines were reactivated, and cell lysates were probed with ORF57- or K_v1.3-specific antibodies and GAPDH used as a measure of equal loading (n=3 biologically independent samples).

(I) Control and K_v1.3-depleted cell lines were reactivated, prior to the culture medium being incubated for with HEK-293T cells. Relative *ORF57* transcript levels were analysed from total RNA by qRT-PCR using GAPDH as a reference, n=3 biological replicates. Significance was calculated using an unpaired Student's t-test, *** = $p<0.001$.

(J) Confocal imaging. Control, K_v1.3-depleted or K_v1.3-rescued cell lines were reactivated , prior to the culture medium being incubated with HEK-293T cells. Cells were then probed with a LANA-specific antibody and stained with DAPI (n=3 biologically independent samples). Scale bars represent 10 µm.

Figure. 2. Increased K^+ currents during lytic KSHV replication is dependent on K_v1.3 expression.

(A-B) TREx BCBL1-RTA cells remained unreactivated or were reactivated with doxycycline hyclate. (Ai) Relative *K_v1.3* transcript levels were analysed from total RNA by qRT-PCR using GAPDH as a reference, n=3 biological replicates. Significance was calculated using an unpaired Student's t-test, *** =

p<0.001. (Aii) Cell lysates were probed with K_v1.3 and ORF57-specific antibodies and GAPDH used as a measure of equal loading (n=3 biological replicates). (B) Relative *KCa3.1* transcript levels were analysed from total RNA by qRT-PCR using GAPDH as a reference, n=3 biological replicates. Significance was calculated using an unpaired Student's t-test, *** = p<0.001.

(C-D) Mean current density voltage relationships for K^+ currents (n=5 for all populations) from (C) unreactivated and reactivated TREx BCBL1-RTA; cells were pre-treated for 24 hours with DMSO or ShK-Dap[22] and (D) Control and K_v1.3-depleted cells lines remained unreactivated or were reactivated with doxycycline hyclate. Significance was calculated using an unpaired Student's t-test, ** = p<0.01, *** = p<0.001, to each corresponding latent control.

(E) Pooled data of resting membrane potentials in latent and lytic TREx BCBL1-RTA cells or control and K_v1.3-depleted cells lines (n=5 biologically independent samples). Significance was calculated using an unpaired Student's t-test, *** = p<0.001, to each corresponding latent control.

(F) Membrane polarisation of TREx BCBL1-RTA cells after incubation with DiBAC4(3) in control and K_v1.3-depleted cells lines (n=3 biologically independent samples). Significance was calculated using a one-way unpaired ANOVA corrected for multiple comparisons using Tukey's multiple comparison test to each latent control, * = p<0.05, *** p<0.001.

Figure 3. KSHV RTA upregulates K_v1.3 expression.

(A-C) A549 and U87 cells transfected with either (A) GFP, RTA-GFP or ORF57–GFP expression constructs, (B) Dose-dependent increase of RTA-GFP or (C) GFP, RTA-GFP or ORF57–GFP in the presence of Mithramycin A. Relative *K_v1.3* or *IL-6* transcript levels were analysed from total RNA by qRT-PCR using GAPDH as a reference, n=3 biologically independent samples. Significance was calculated using a one-way unpaired ANOVA corrected for multiple comparisons using Tukey's multiple comparison test, * = p<0.05, ** = p<0.01, *** p<0.001.

(D) ChIP assays of unreactivated versus reactivated TREx BCBL1-RTA cells using antibodies specific to SP-1, RNAPII, myc-RTA or mouse and rabbit IgG control antibodies. PCR amplification was performed

on the immunoprecipitates using $K_v1.3$ promoter specific primers, n=3 biologically independent samples. Significance was calculated using an unpaired Student's t-test, * = p<0.05.

Figure 4. Ca^{2+} influx is essential during KSHV lytic replication and sufficient to override the effect of $K_v1.3$ knockdown.

(A) Fura Red staining of calcium ratios from control and $K_v1.3$-depleted TREx BCBL1-RTA cells, calcium ionophore A23187 was used as a positive control (n=3 biologically independent samples). Significance was calculated using a one-way unpaired ANOVA corrected for multiple comparisons using Tukey's multiple comparison test, * = p<0.05, *** p<0.001.

(B) TREx BCBL1-RTA cells pretreated with EGTA prior to reactivation, then probed with RTA-specific antibodies and stained with DAPI post reactivation (n=3 biologically independent samples). Scale bars represent 5 μm.

(C) TREx BCBL1-RTA cells were pretreated with EGTA prior to reactivation. Relative *ORF57* transcript levels were analysed from total RNA by qRT-PCR, using GAPDH as a reference, n=3 biologically independent samples. Significance was calculated using an unpaired Student's t-test, *** = p<0.001.

(D) TREx BCBL1-RTA cells remained unreactivated or reactivated in the absence or presence of A23187. Cell lysates were probed with Myc- or ORF57-specific antibodies and GAPDH used as a measure of equal loading (n=3 biologically independent samples).

(E) $K_v1.3$-depleted TREx BCBL1-RTA cells remained unreactivated or reactivated in the absence or presence of A23187. Cell lysates were probed with Myc- or ORF57-specific antibodies and GAPDH used as a measure of equal loading (n=3 biologically independent samples).

Figure 5. KSHV-mediated calcium influx initiates NFAT1 nuclear localisation and NFAT1-mediated gene expression.

(A-B) TREx BCBL1-RTA cells remained unreactivated or were pre-treated with non-cytotoxic dose-dependent concentrations of (A) CsA and (B) VIVIT prior to reactivation with doxycycline hyclate. Cell

682 lysates were probed with ORF57-specific antibody, GAPDH was used as a measure of equal loading
683 (n=3 biologically independent samples).
684 (C) Confocal imaging. TREx BCBL1-RTA cells remained unreactivated or were pre-treated with ShK-
685 Dap[22] or CsA prior to reactivation. Cells were then probed with NFAT1 or ORF57-specific antibodies
686 and stained with DAPI (n=3 biologically independent samples). Scale bars represent 5 μm.
687 (D) Relative NFAT-responsive transcript levels analysed from total RNA from unreactivated and
688 reactivated control and K_v1.3-depleted cell lines, by qRT-PCR from total RNA using GAPDH as a
689 reference. n=3 biologically independent samples. Significance was calculated using an unpaired
690 Student's t-test, * = $p<0.05$.
691
692 **Figure 6. K_v1.3 is a direct contributor to KSHV lytic replication in B cells.**
693 Schematic representation of the KSHV-mediated K_v1.3 induced hyperpolarisation and calcium influx
694 mechanism required for efficient lytic replication. Potential therapeutic interventions are
695 highlighted. Created with Biorender.com.

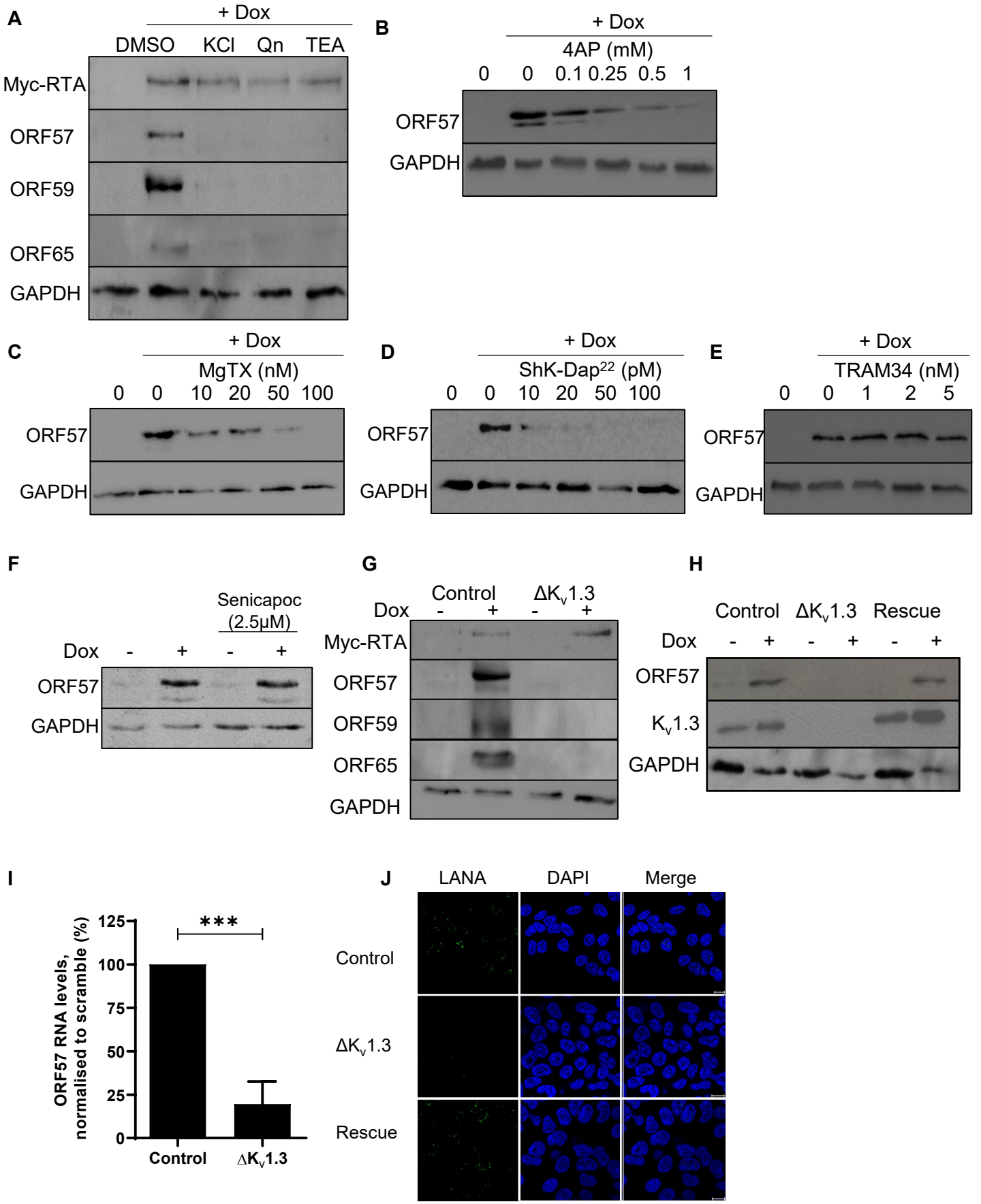
A
+ Dox
DMSO
KCl
Qn
TEA
Myc-RTA
ORF57
ORF59
ORF65
GAPDH
B
+ Dox
4AP (mM)
0 0 0.1 0.25 0.5 1
ORF57
GAPDH
C
+ Dox
MgTX (nM)
0 0 10 20 50 100
ORF57
GAPDH
D
+ Dox
ShK-Dap22 (pM)
0 0 10 20 50 100
ORF57
GAPDH
E
+ Dox
TRAM34 (nM)
0 0 1 2 5
ORF57
GAPDH
F
Senicapoc (2.5μM)
Dox - + - +
ORF57
GAPDH
G
Control
ΔKv1.3
Dox - + - +
Myc-RTA
ORF57
ORF59
ORF65
GAPDH
H
Control
ΔKv1.3
Rescue
Dox - + - + - +
ORF57
Kv1.3
GAPDH
I
ORF57 RNA levels, normalised to scramble (%)
125
100
75
50
25
0
***
Control
ΔKv1.3
J
LANA
DAPI
Merge
Control
ΔKv1.3
Rescue

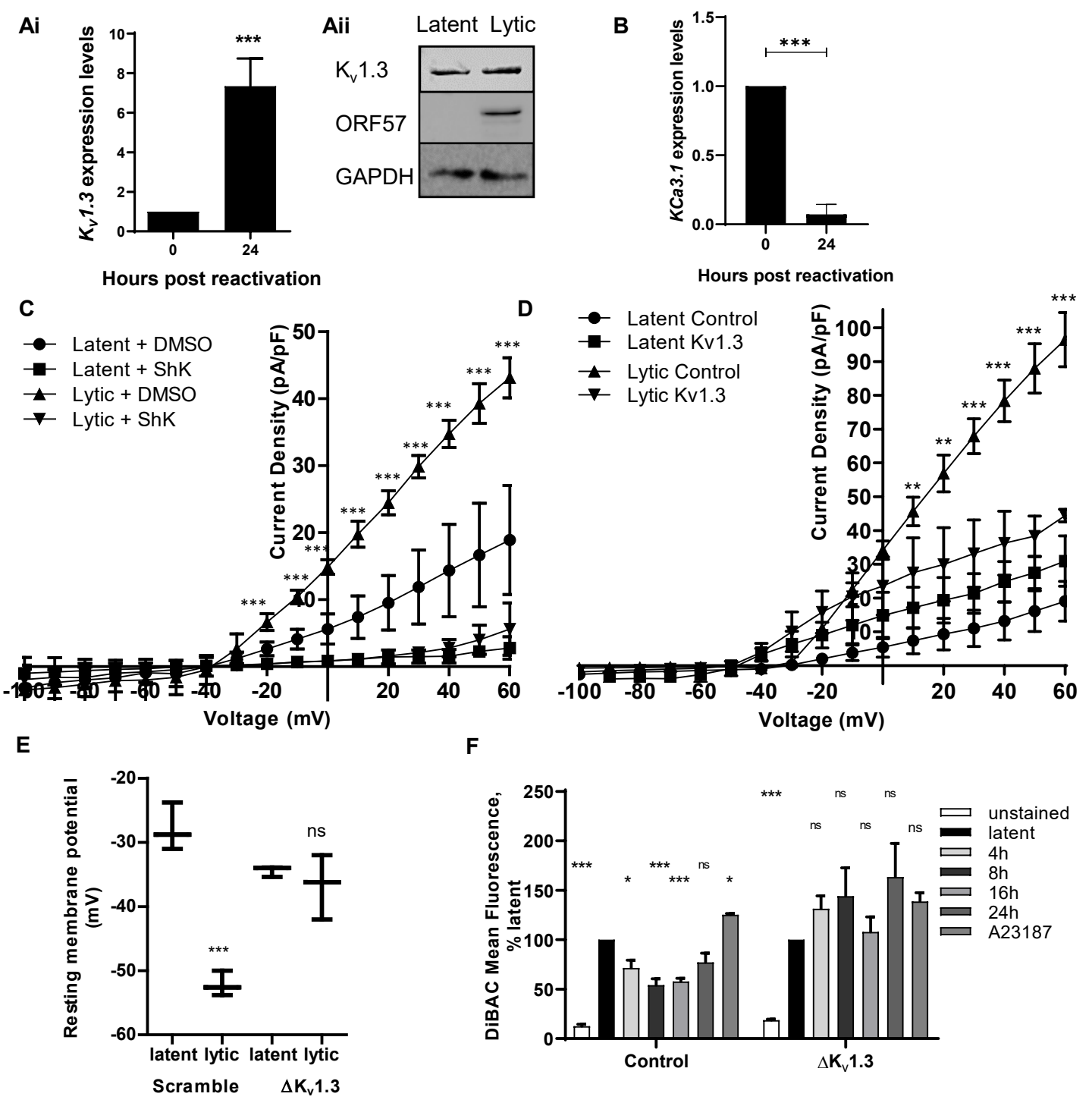
Ai
Kv1.3 expression levels
Hours post reactivation
Aii
Latent Lytic
Kv1.3
ORF57
GAPDH
B
KCa3.1 expression levels
Hours post reactivation
C
Latent + DMSO
Latent + ShK
Lytic + DMSO
Lytic + ShK
Current Density (pA/pF)
Voltage (mV)
D
Latent Control
Latent Kv1.3
Lytic Control
Lytic Kv1.3
Current Density (pA/pF)
Voltage (mV)
E
Resting membrane potential (mV)
latent lytic latent lytic
Scramble
ΔKv1.3
F
DiBAC Mean Fluorescence, % latent
unstained
latent
4h
8h
16h
24h
A23187
Control
ΔKv1.3

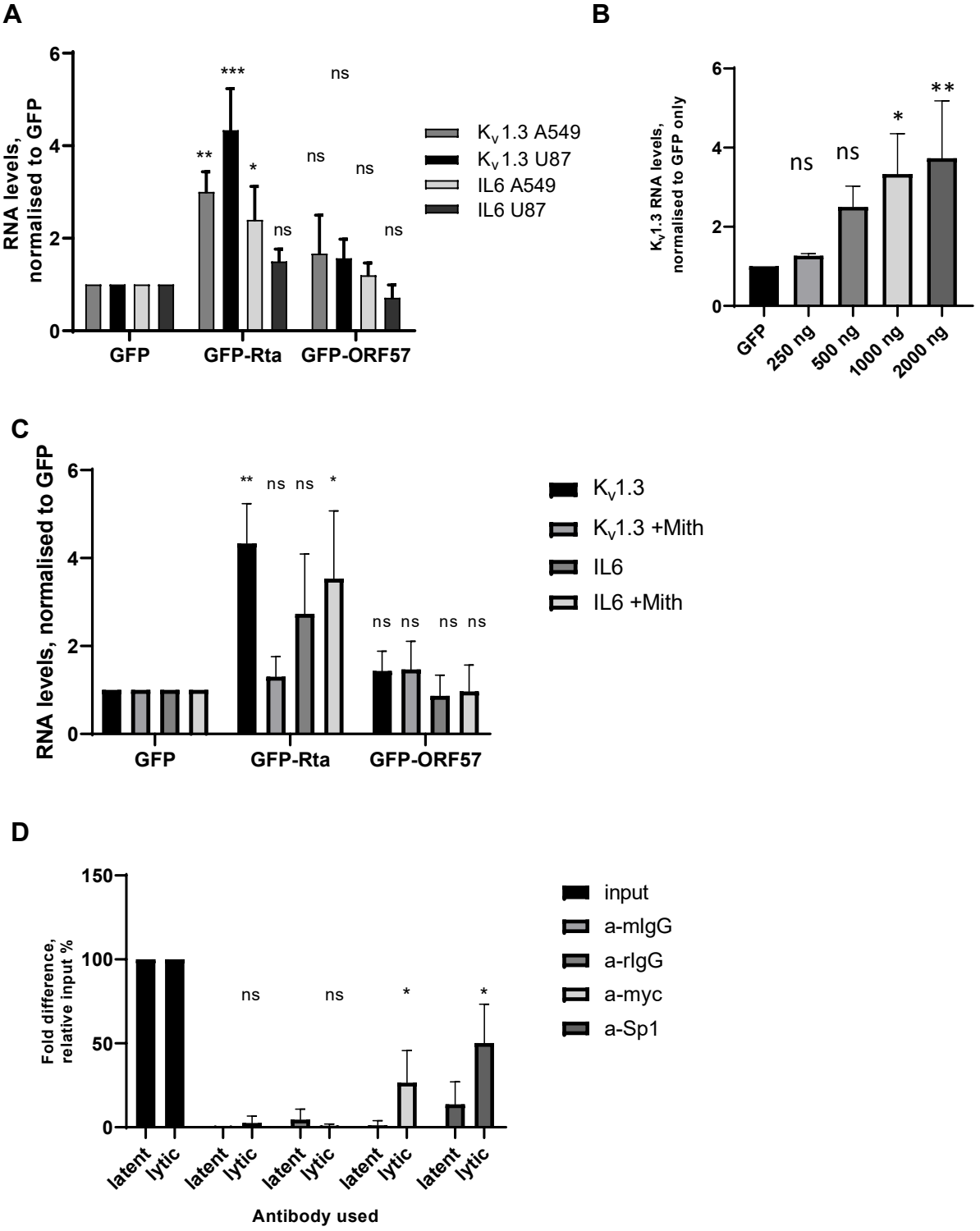
A
RNA levels, normalised to GFP
6
4
2
0
**
***
*
ns
ns
ns
ns
ns
GFP
GFP-Rta
GFP-ORF57
K_v1.3 A549
K_v1.3 U87
IL6 A549
IL6 U87
B
K_v1.3 RNA levels, normalised to GFP only
ns
ns
*
**
GFP
250 ng
500 ng
1000 ng
2000 ng
C
RNA levels, normalised to GFP
**
ns
ns
*
ns
ns
ns
ns
GFP
GFP-Rta
GFP-ORF57
K_v1.3
K_v1.3 +Mith
IL6
IL6 +Mith
D
Fold difference, relative input %
150
100
50
0
ns
ns
*
*
latent
lytic
Antibody used
input
a-mIgG
a-rIgG
a-myc
a-Sp1

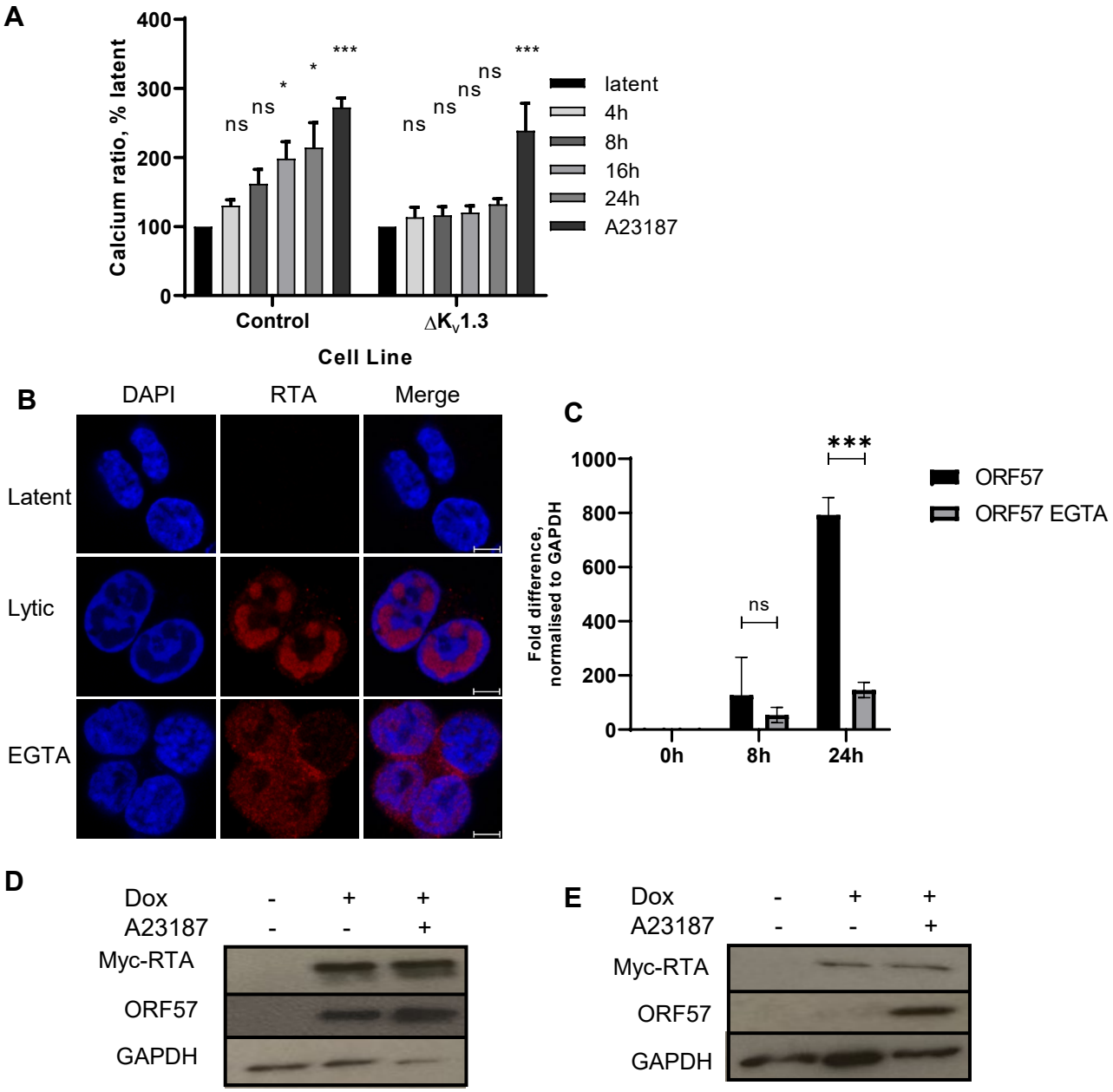
A
Calcium ratio, % latent
400
300
200
100
0
ns
ns
*
*
***
ns
ns
ns
***
latent
4h
8h
16h
24h
A23187
Control
ΔKV1.3
Cell Line
B
DAPI
RTA
Merge
Latent
Lytic
EGTA
C
Fold difference, normalised to GAPDH
1000
800
600
400
200
0
ns
***
ORF57
ORF57 EGTA
0h
8h
24h
D
Dox - + +
A23187 - - +
Myc-RTA
ORF57
GAPDH
E
Dox - + +
A23187 - - +
Myc-RTA
ORF57
GAPDH

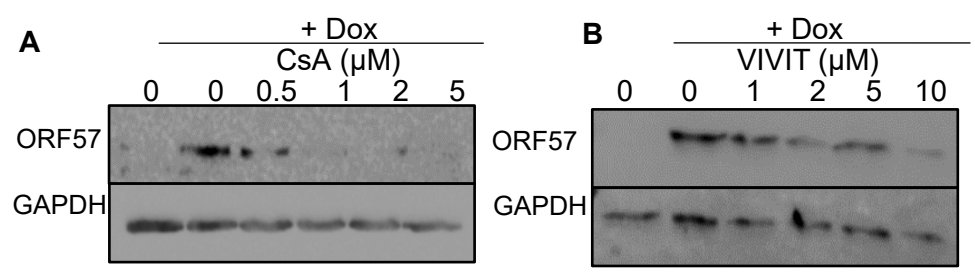
A
+ Dox
CsA (μM)
0 0 0.5 1 2 5
ORF57
GAPDH
B
+ Dox
VIVIT (μM)
0 0 1 2 5 10
ORF57
GAPDH

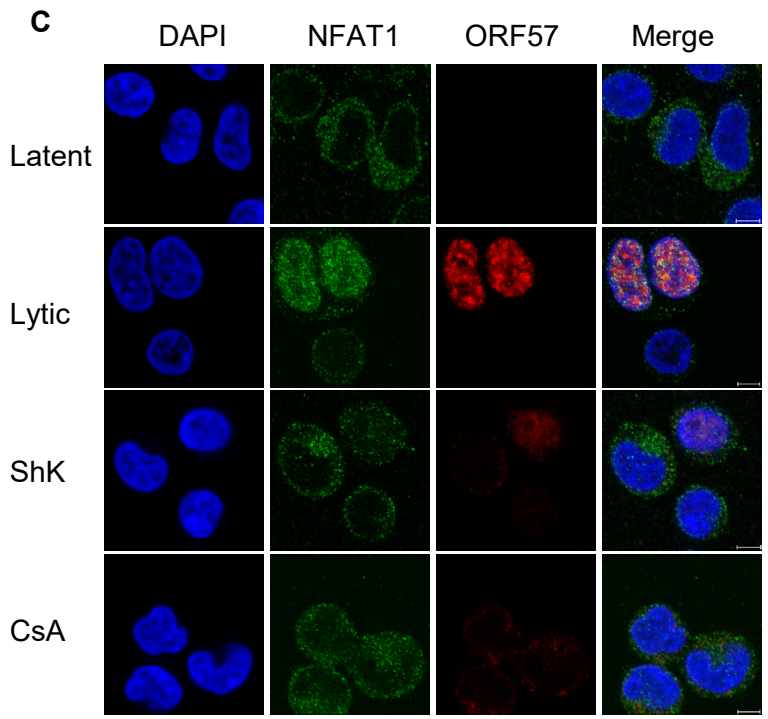
C
DAPI
NFAT1
ORF57
Merge
Latent
Lytic
ShK
CsA

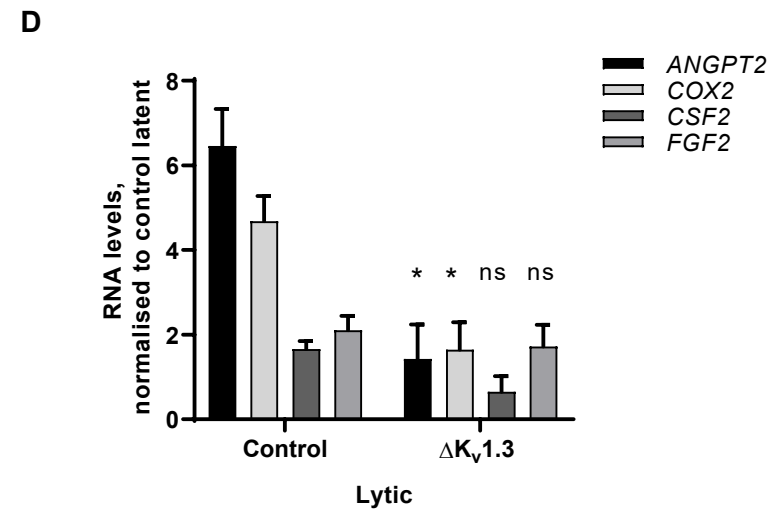
D
ANGPT2
COX2
CSF2
FGF2
RNA levels, normalised to control latent
0
2
4
6
8
* * ns ns
Control
ΔKv1.3
Lytic

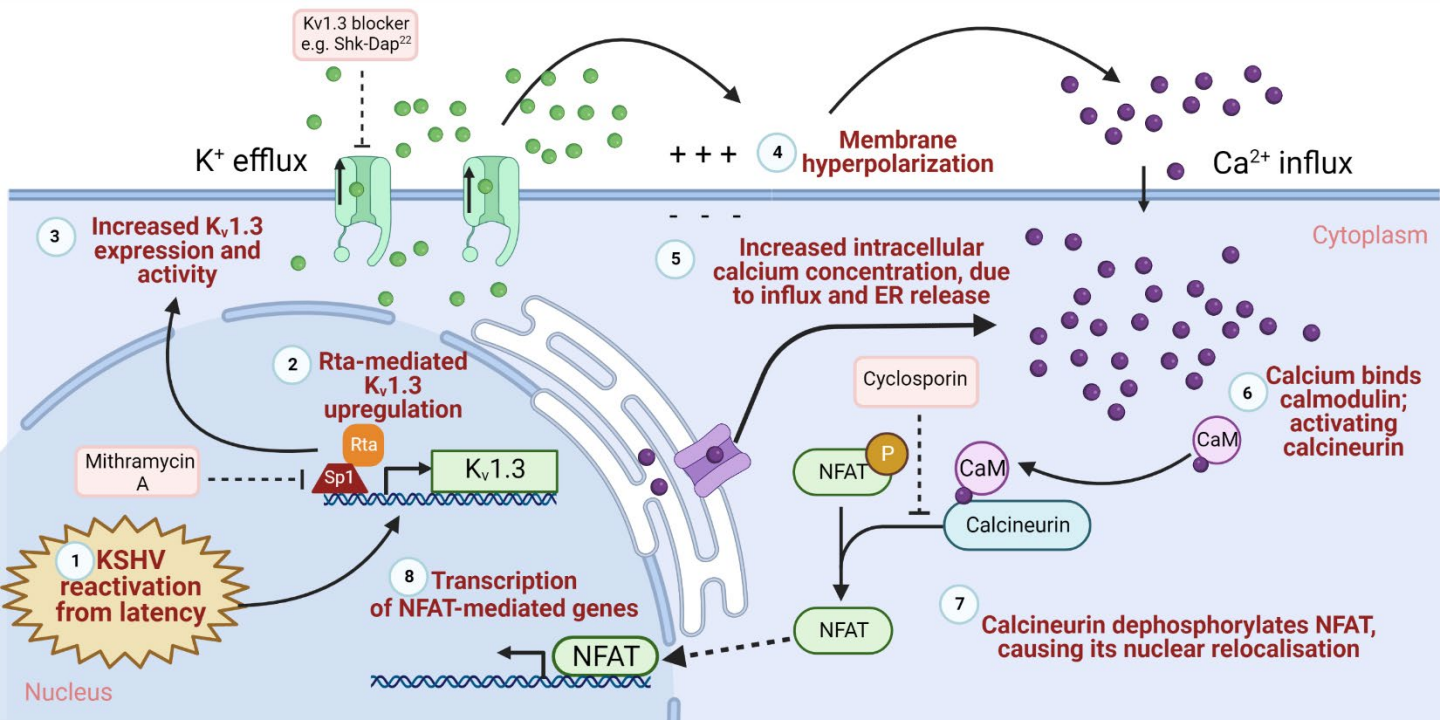
Kv1.3 blocker
e.g. Shk-Dap22
K+ efflux
+ + +
4 Membrane hyperpolarization
Ca2+ influx
3 Increased Kv1.3 expression and activity
5 Increased intracellular calcium concentration, due to influx and ER release
Cytoplasm
2 Rta-mediated Kv1.3 upregulation
Rta
Sp1
Kv1.3
Mithramycin A
Cyclosporin
6 Calcium binds calmodulin; activating calcineurin
CaM
NFAT
P
CaM
Calcineurin
1 KSHV reactivation from latency
8 Transcription of NFAT-mediated genes
NFAT
NFAT
7 Calcineurin dephosphorylates NFAT, causing its nuclear relocalisation
Nucleus